Photonic Hook-Assisted Contrast-Enhanced Super-Resolution Imaging Using Janus Microspheres

Pengxin Zou, Chu Xu, Lingjie Zhi, Sorin Melinte, Zengbo Wang, Chao Zuo, *Senior Member, IEEE*, and Ran Ye

***Abstract*— Microsphere-assisted imaging is a promising label-free super-resolution imaging technique. Its performance is significantly affected by the photonic nanojet (PNJ) of microspheres. Recently, a new type of curved PNJ, i.e. the photonic hook (PH), was discovered, which shows promising potential for various applications. This Letter presented a contrast-enhanced super-resolution imaging technique utilizing the PHs generated by Janus microspheres. We demonstrated that the Janus microspheres can be fabricated using a one-step deposition process, they exhibit superior imaging performance to pristine microspheres, and their field-of-view and imaging contrast can be easily adjusted by changing the coating thickness. In addition, we demonstrated that the imaging contrast of Janus microspheres can be further enhanced by using polarized illumination.**

***Index Terms*— Super-resolution imaging, microspheres, patchy microsphere, photonic nanojet, photonic hook.**

I. Introduction

MICROSPHERE-ASSISTED imaging is a label-free super-resolution microscopic method that helps conventional optical microscopes overcome their resolution limits and observe smaller details in samples. This technique was first proposed by Wang et al. [1] and quickly draw widespread attention due to its unique advantages, such as no need for fluorescent labeling, functional under white light illumination, etc. [2]. To further improve the imaging performance of microspherical lenses, various parameters have been optimized, including the diameter and material of microspheres [3], [4], the immersion environment of microspheres [5], [6], [7] and the illumination condition of imaging systems [8], [9]. Recently, micromachining has emerged as an effective tool to modify the imaging performance of microspheres. For example, in 2022, Wu et al. coated microspheres with dielectric bilayer thin films to eliminate the Newton's ring effect and successfully improved the imaging quality of microspheres [10]. In 2023, focused ion beam milling was used to fabricate hyper-hemi-microsphere lenses, and a resolution of ∼50 nm can be achieved with those reshaped microspheres [11].

Due to the Mie scattering, dielectric microspheres under illumination generate photonic nanojets (PNJs) at their shadow side [12]. It has been demonstrated that the imaging performance of microlenses can be significantly influenced by the effective length, position and full-width-half-maximum (FWHM) of its PNJ. For example, Yang et al. found that reducing the FWHM of PNJ can enhance the resolution of microspheres [13]. The length of the PNJ is also demonstrated to be influential to the depth of view of the microspheres [4]. In 2018, a new type of PNJ with a curved structure, i.e. the photonic hook (PH), was reported [14]. The formation mechanism of PHs can be attributed to the combined effects of the phase velocity difference and interference of propagating waves. Both anistropic particles and non-uniform illumination are suitable for PH generation. For instance, patchy microspheres with metallic surface coatings can block a portion of incoming light, resulting in an asymmetric illumination effect. Their capacity of PH generation has been theoretically and experimentally demonstrated [15], [16], [17]. One of the most important applications of PHs is in super-resolution imaging [18], [19]. In 2021, Shang et al. deposited silver films onto self-assembled hexagonally-closed-packed (hcp) microsphere arrays, and successfully performed super-resolution imaging with those patchy microspheres [18]. Nevertheless, due to the inherent defects arising from the self-assembly process, it is still challenging to well control the morphology of patchy microspheres. Janus particles, named after the double-faced Roman god, are particles with two sides of different physical or chemical properties. Due to their simple surface morphology, Janus particles can be fabricated in a controlled manner by various methods, making them a promising alternative to address the aforementioned shortcoming [20].

Manuscript received 12 November 2023; revised 3 January 2024; accepted 13 January 2024. Date of publication 22 January 2024; date of current version 5 February 2024. This work was supported in part by the National Natural Science Foundation of China under Grant 62105156, in part by the National Key Research and Development Program of China under Grant 2022YFA1205002, in part by Belgian Fonds de la Recherche Scientifique—FNRS under Grant T.0126.22 and Grant U.N027.18, in part by the Leverhulme Trust under Grant RF-2022-659, and in part by the Royal Society under Grant IEC\R2\202178. *(Corresponding author: Ran Ye.)*

Pengxin Zou, Chu Xu, Lingjie Zhi, and Ran Ye are with the School of Computer and Electronic Information, Nanjing Normal University, Nanjing 210023, China (e-mail: ran.ye@njnu.edu.cn).

Sorin Melinte is with the Institute of Information and Communication Technologies, Electronics and Applied Mathematics, Université Catholique de Louvain, 1348 Louvain-la-Neuve, Belgium.

Zengbo Wang is with the School of Computer Science and Electronic Engineering, Bangor University, LL57 1UT Bangor, U.K.

Chao Zuo is with the Smart Computational Imaging Laboratory (SCILab), School of Electronic and Optical Engineering, Nanjing University of Science and Technology, Nanjing 210094, China.

Color versions of one or more figures in this letter are available at https://doi.org/10.1109/LPT.2024.3356718.

Digital Object Identifier 10.1109/LPT.2024.3356718

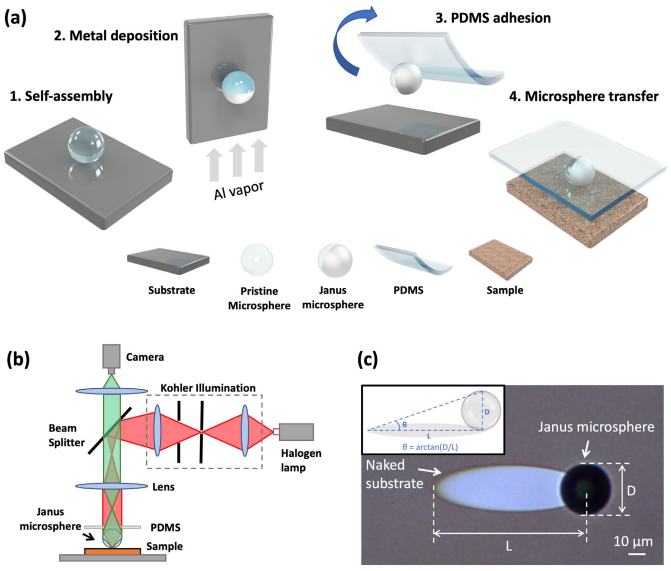

Fig. 1. (a) Illustrative drawings of the fabrication and manipulation of Janus microspheres; (b) Schematic drawing of the microsphere-assisted microscopic imaging system; (c) Optical picture of a Janus microsphere after Al deposition.

II. Results and Discussion

A. Materials and Methods

In this study, Janus microspheres were fabricated from barium titanate glass ($BaTiO_3$, BTG) particles with a refractive index of ∼1.90, which were supplied by the Microspheres-Nanospheres (New York, USA) as powders. The mean diameter of the BTG microsphere is ∼30 μm. As shown in Fig. 1 (a), to fabricate Janus microspheres, we first drop-casted a small amount of BTG particles onto a glass slide, and then deposited aluminum films of different thickness (5 - 100 nm) onto the side of BTG particles through the glancing angle deposition method [21]. The deposition rate was kept constant at 1 Å/s during deposition, and a homemade rotation stage was made to control the deposition angle (θ). After deposition, a transparent polydimethylsiloxane (PDMS, ∼ 1 mm thick) film was gently pressed onto the glass slide. Due to the van dear Waals forces, the Janus microspheres were bonded to the PDMS film, and detached from the glass slide when the PDMS film was lifted. Then, we directed the Janus microspheres to the region of interest by manipulating the PDMS film with a homemade holder positioned under an objective lens. The Janus microspheres worked in the contact mode and formed a real image above the sample surface [22].

As shown in Fig. 1 (b), the super-resolution imaging experiments were performed using a commercial reflection optical microscope (Axio AX10, Carl Zeiss). White-light illumination with a peak wavelength of 550 nm was provided by a halogen lamp (HAL 100, Carl Zeiss). The objective lens used (EC EPIPLAN, Carl Zeiss) has a magnification factor of 100× and a numerical aperture (NA) of 0.9. The samples were observed in air using the bright-field imaging mode. A high-speed scientific complementary metal oxide semiconductor (CMOS) camera (DFC295, Leica) was employed to capture optical images for subsequent analysis.

Figure 1 (c) shows the optical microscopic (OM) picture of a Janus microsphere after Al deposition. During the deposition process, the microsphere serves as a mask, blocking the transportation of aluminum vapors from the source to the substrate. Consequently, the area in the shadow of the microsphere remains unmetallized. The elliptical pattern on the substrate, indicated by a white arrow, represents this unmetallized area. The inset of Fig. 1 (c) demonstrates how the deposition angle (θ) can be determined using the equation $\theta = arctan(D/L)$, where D denotes the diameter of the microsphere, and L corresponds to the length of the elliptical structure.

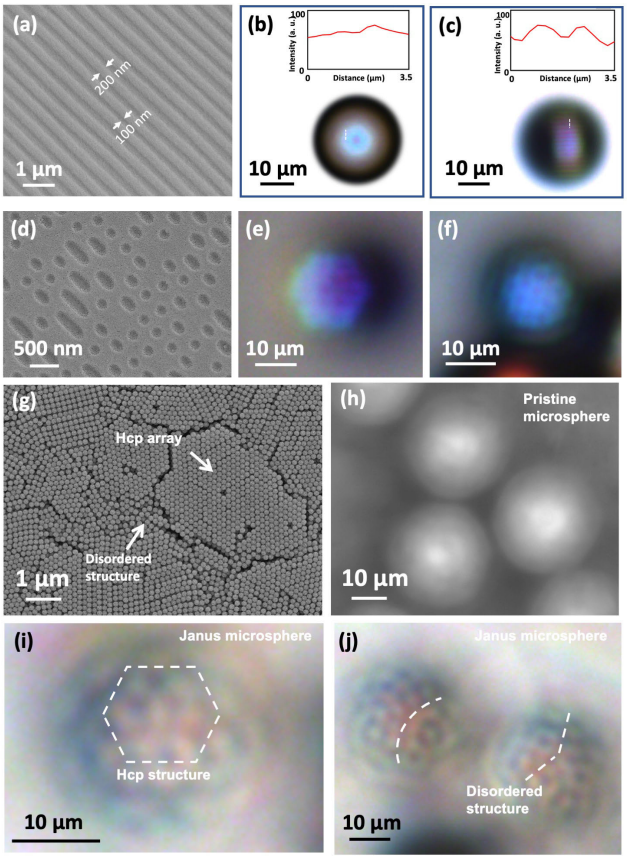

Fig. 2. (a) Scanning electron microscopic (SEM) image of a BD; (b), (c) OM pictures of the BD observed through (b) a pristine microsphere and (c) a Janus microsphere; (d) SEM image of a BD with data pits; (e), (f) OM pictures of the BD with data pits observed through (e) a pristine microsphere and (f) a Janus microsphere; (g) SEM image of silica particle arrays; (h)-(j) OM pictures of the particle arrays observed through (h) pristine microspheres and (i), (j) Janus microspheres.

B. Comparison Between Pristine and Janus Microsphere

Then, we compared the imaging performance of pristine and Janus microspherical lenses, blank Blu-ray Discs (BDs) with grating structures were used as observation samples. Figure 2 (a) is the scanning electron microscopic (SEM) image of a blank BD, which shows a stripe pattern with 300 nm periodicity, including 200 nm track width and 100 nm gap between adjacent tracks. As shown in Fig. 2 (b), the stripe patterns imaged by the pristine microspheres have a low contrast and can hardly be seen. In contrast, we found that the use of Janus microspheres can significantly improve the imaging quality. Figure 2 (c) is the stripe patterns observed through a Janus microsphere deposited with 40 nm-thick Al films, which have a sharper appearance and a higher contrast compared to

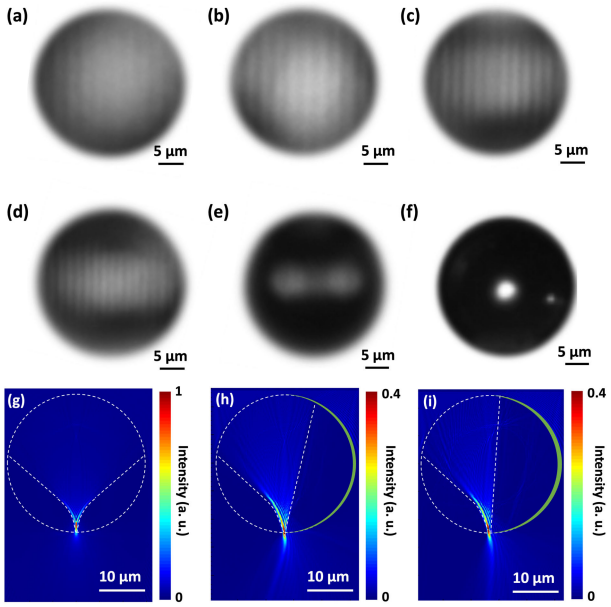

Fig. 3. (a)-(f) OM images of Janus microspheres coated with different thickness of Al films. The film thickness is (a) 0 nm, (b) 20 nm, (c) 30 nm, (d) 40 nm, (e) 80 nm and (f) 100 nm, respectively; (g) Simulated light field generated by a pristine microsphere; (h), (i) Simulated light fields generated by Janus microspheres with (h) 30 nm- and (i) 80 nm-thick Al films (green lines).

those taken with pristine microspheres. This improvement in imaging contrast is further supported by the intensity profiles extracted along the dashed lines in Figs. 2 (b) and (c).

It is reported that microspherical lenses have a poorer imaging performance when observing non-periodic microstructures [23]. To study the influence of sample periodicity, we used Janus microspheres to observe a data-encoded BD substrate. As shown in Fig. 2 (d), there are pit arrays with a non-periodical arrangement on the surface of the encoded BD, the smallest pit size is $\sim$ 150 nm. Figures 2 (e), (f) are the pit arrays observed through pristine and Janus microspheres, respectively. The Janus spherical lens once again shows a better imaging contrast than its pristine counterpart.

Then, we fabricated 150 nm-diameter SiO_2 particle arrays from colloidal suspensions (Bangs Laboratory, USA) by the gravity-assisted self-assembly method [24]. The particle arrays were deposited with 10 nm Al film to enhance their optical reflectance before use. Figure 2 (g) is the SEM image of the prepared sample, which shows the presence of both highly ordered hcp structures and disordered structures. We found that the prepared sample is beyond the resolution of pristine microspheres [Fig. 2 (h)], while its microstructure can be clearly distinguished by the Janus microspheres under the same observation condition [Figs. 2 (i), (j)]. The structural variations of the sample, i.e. the hcp and disordered arrangement, can be observed with the help of Janus microspheres, as indicated by the dashed lines representing the arrangement of silica particles in Figs. 2 (i), (j).

C. Influence of Film Thickness on the Imaging Performance of Janus Microspheres

The aperture is one of the most important parameters in optical designs. In this Letter, we showed that by changing the thickness of Al films, Janus microspheres with different apertures can be obtained. To demonstrate this, we fabricated 30 μm-diameter Janus microspheres by depositing Al film of different thickness onto BTG microspheres at a constant deposition angle of $\theta \sim 5°$. Then, the prepared Janus microspheres were positioned on a BD substrate. The Al coating functions like an aperture stop by reflecting the incident light backwards and preventing it from entering the microsphere. As shown in Figs. 3 (a)-(d), increasing the thickness of Al films from 0 to 40 nm results in an enhancement of imaging contrast. The imaging contrast begins to deteriorate when the Al film is increased to 80 nm [Fig. 3 (e)]. The Janus microspheres completely lose their imaging capability when the film thickness reaches 100 nm [Fig. 3 (f)]. Furthermore, we found that the field-of-view (FOV) of the microspherical lenses also can be effectively adjusted by changing the film thickness. Janus microspheres with thicker Al films tend to have a smaller FOV, as shown in Figs. 3 (a)-(f).

We then used the Finite-Difference Time-Domain (FDTD) method to investigate the light focusing performance of microspherical lenses. As shown in Fig. 3 (g), a pristine microsphere in air generates a symmetrical light field whose $|E|^2$ intensity is mirrored along the propagation direction of incident light. However, this symmetry is broken in Janus microspheres. As shown in Fig. 3 (h), the microsphere coated with 30 nm Al films generates a curved $|E|^2$ intensity distribution, i.e. a PH, on its shadow side. The degree of asymmetry becomes higher when the thickness of Al films increases to 80 μm [Fig. 3 (i)]. The formed PHs then enhance the imaging contrast of Janus microspheres by creating an asymmetric illumination condition on sample surface. Asymmetric illumination or oblique illumination is a commonly used contrast enhancement technique in optical microscopy [25]. Under this illumination condition, the details of the BD sample becomes more visible as the intensity difference of the light reflected by the track pitch and the base substrate is increased due to the shadowing effect caused by the variations in the vertical dimension of structures.

D. Contrast Enhancement by Polarized Illumination

Polarized light microscopy is a conventional contrast-enhancing technique for birefringent materials. Nonetheless, its utilization in microsphere-assisted imaging is still at early stage. In 2021, Johnson et al. reported the use of polarized PNJ generated by pristine microspheres for the super-resolution imaging of collagen architecture [26]. In this study, we show that using polarized light illumination can effectively generate polarized PHs and significantly enhance the imaging contrast of Janus microspheres for birefringent materials. To the best of our knowledge, this is the first report of super-resolution imaging based on polarized PHs. As shown in Fig. 4 (a), we integrated a Janus microsphere into a conventional reflected light microscope equipped with a polarizer and a analyzer. BDs were used for observation because they can be considered as an artificial birefringent material due to their grating structures [27]. The BTG microsphere has a diameter of 30 μm and it is coated with 30 nm-thick Al films on its side. The

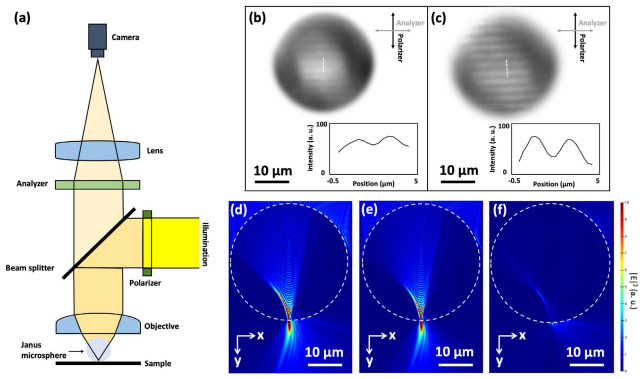

Fig. 4. (a) Schematic drawing of the microsphere-integrated polarized imaging system; (b), (c) OM images of Janus microspheres under (b) non-polarized and (c) polarized illumination; (d) The simulated electric field generated by the Janus microsphere; (e) The x-component of the electric field intensity; (f) Subtraction of the x-component from the total field.

polarizing axis of the illumination was kept perpendicular to the grating pattern, while the orientation of analyzer was changed. We found that the best imaging contrast was obtained when the analyzer was oriented at 90° with respect to the polarizer (Fig. S1), indicating that the state of polarization was altered by the structures during the reflection process. Figure 4 (b) is the sample imaged by the Janus microsphere under non-polarized illumination, while Fig. 4 (c) is the same region observed under polarized illumination. The axes of the polarizer and analyzer are shown in the picture. We can easily notice an improvement in the imaging contrast with a value of ∼2.8 times higher when polarization is applied. The contrast was obtained by the equation of $contrast = \frac{I_{max}-I_{min}}{I_{max}+I_{min}}$. Then, we used the FDTD method to study the PHs formed by Janus microspheres under polarized illumination. As shown in Figs. 4 (d)-(f), the simulation was performed with plane waves polarized along the X-axis and propagating along the Y-axis. The waves are focused into PHs at the shadow side of the Janus microspheres. We found that the x-component of the electrical field intensity (E_x^2) is much stronger than the electrical field intensity obtained by subtracting the x-component from the total field (E^2 - E_x^2), which indicates that the polarization state of incident light is not significantly affected when focused into a PH.

III. Conclusion

In conclusion, we have proposed a contrast-enhanced super-resolution imaging technique utilizing the PHs generated by Janus microspheres. The Janus microspheres can be easily fabricated by a one-step deposition method. We have demonstrated that the Janus microspheres have a better imaging performance than pristine microspheres. By adjusting the coating thickness, we can easily design the FOV and imaging contrast of Janus microspheres. Furthermore, for the first time, we have shown that using polarized illumination can significantly enhance the imaging contrast of Janus microspheres due to the formation of polarized PHs.

References

[1] Z. Wang et al., "Optical virtual imaging at 50 nm lateral resolution with a white-light nanoscope," *Nature Commun.*, vol. 2, no. 1, p. 218, Mar. 2011.

[2] L. Chen, Y. Zhou, Y. Li, and M. Hong, "Microsphere enhanced optical imaging and patterning: From physics to applications," *Appl. Phys. Rev.*, vol. 6, no. 2, Apr. 2019, Art. no. 021304.

[3] Y. Xie et al., "Chalcogenide microsphere-assisted optical super-resolution imaging," *Adv. Opt. Mater.*, vol. 10, no. 6, Jan. 2022, Art. no. 2102269.

[4] S. Yang et al., "Influence of the photonic nanojet of microspheres on microsphere imaging," *Opt. Exp.*, vol. 25, no. 22, pp. 27551–27558, Oct. 2017.

[5] R. Ye et al., "Experimental imaging properties of immersion microscale spherical lenses," *Sci. Rep.*, vol. 4, no. 1, p. 3769, Jan. 2014.

[6] F. Wang et al., "Microsphere-assisted super-resolution imaging with enlarged numerical aperture by semi-immersion," *Appl. Phys. Lett.*, vol. 112, no. 2, Jan. 2018, Art. no. 023101.

[7] A. Darafsheh, "Influence of the background medium on imaging performance of microsphere-assisted super-resolution microscopy," *Opt. Lett.*, vol. 42, no. 4, pp. 735–738, Feb. 2017.

[8] S. Perrin, H. Li, A. Leong-Hoi, S. Lecler, and P. Montgomery, "Illumination conditions in microsphere-assisted microscopy," *J. Microsc.*, vol. 274, no. 1, pp. 69–75, Apr. 2019.

[9] S. Perrin et al., "Transmission microsphere-assisted dark-field microscopy," *Phys. Status Solidi RRL*, vol. 13, Oct. 2018, Art. no. 1800445.

[10] G. Wu, Y. Zhou, and M. Hong, "Bilayer-film-decorated microsphere with suppressed interface reflection for enhanced nano-imaging," *Opt. Exp.*, vol. 30, no. 16, pp. 28279–28289, Jul. 2022.

[11] G. Wu, Y. Zhou, and M. Hong, "Sub-50 nm optical imaging in ambient air with 10x objective lens enabled by hyper-hemi-microsphere," *Light, Sci. Appl.*, vol. 12, no. 1, p. 49, Feb. 2023.

[12] B. S. Luk'yanchuk, R. Paniagua-Domínguez, I. Minin, O. Minin, and Z. Wang, "Refractive index less than two: Photonic nanojets yesterday, today and tomorrow," *Opt. Mater. Exp.*, vol. 7, pp. 1820–1847, May 2017.

[13] H. Yang, R. Trouillon, G. Huszka, and M. A. M. Gijs, "Super-resolution imaging of a dielectric microsphere is governed by the Waist of its photonic nanojet," *Nano Lett.*, vol. 16, no. 8, pp. 4862–4870, Jul. 2016.

[14] L. Yue, O. V. Minin, Z. Wang, J. N. Monks, A. S. Shalin, and I. V. Minin, "Photonic hook: A new curved light beam," *Opt. Lett.*, vol. 43, no. 4, pp. 771–774, Feb. 2018.

[15] F. Tang et al., "Generation of photonic hooks from patchy microcylinders," *Photonics*, vol. 8, no. 11, p. 466, Oct. 2021.

[16] Q. Shang et al., "Generation of photonic hooks under point-source illumination from patchy microcylinders," *Photonics*, vol. 9, p. 667, Sep. 2022.

[17] C. Xu et al., "Focusing light with a metal film coated patchy particle," *Opt. Exp.*, vol. 31, no. 6, pp. 10894–10904, Mar. 2023.

[18] Q. Shang et al., "Super-resolution imaging with patchy microspheres," *Photonics*, vol. 8, no. 11, p. 513, Nov. 2021.

[19] O. V. Minin and I. V. Minin, "Terahertz microscope with oblique sub-wavelength illumination: Design principle," *Quantum Electron.*, vol. 52, no. 1, pp. 13–16, Jan. 2022.

[20] J. Hu, S. Zhou, Y. Sun, X. Fang, and L. Wu, "Fabrication, properties and applications of Janus particles," *Chem. Soc. Rev.*, vol. 41, no. 11, pp. 4356–4378, 2012.

[21] A. B. Pawar and I. Kretzschmar, "Patchy particles by glancing angle deposition," *Langmuir*, vol. 24, no. 2, pp. 355–358, Jan. 2008.

[22] G. Huszka, H. Yang, and M. A. M. Gijs, "Microsphere-based super-resolution scanning optical microscope," *Opt. Exp.*, vol. 25, no. 13, pp. 15079–15092, Jun. 2017.

[23] J. Zang, Y. Pei, S. Yang, Y. Cao, and Y.-H. Ye, "Microsphere-assisted imaging of periodic and non-periodic structures," *IEEE Photon. Technol. Lett.*, vol. 34, no. 6, pp. 341–344, Mar. 15, 2022.

[24] C. Fang, S. Yang, X. Wang, P. He, R. Ye, and Y.-H. Ye, "Fabrication of two-dimensional silica colloidal crystals via a gravity-assisted confined self-assembly method," *Colloid Interface Sci. Commun.*, vol. 37, Jul. 2020, Art. no. 100286.

[25] C. Sanchez et al., "Oblique illumination in microscopy: A quantitative evaluation," *Micron*, vol. 105, pp. 47–54, Feb. 2018.

[26] P. B. Johnson et al., "Superresolved polarization-enhanced second-harmonic generation for direct imaging of nanoscale changes in collagen architecture," *Optica*, vol. 8, no. 5, pp. 674–685, May 2021.

[27] M. Chen, F. Fan, S.-T. Xu, and S.-J. Chang, "Artificial high birefringence in all-dielectric gradient grating for broadband terahertz waves," *Sci. Rep.*, vol. 6, no. 1, p. 38562, Dec. 2016.